

Article

# Crystal Structure and Supramolecular Architecture of Inorganic Ligand-Coordinated Salen-Type Schiff Base Complex: Insights into Halogen Bond from Theoretical Analysis and 3D Energy Framework Calculations

Qiong Wu <sup>1,2,\*</sup> , Jian-Chang Xiao <sup>1</sup>, Cun Zhou <sup>3</sup>, Jin-Rong Sun <sup>1</sup>, Mei-Fen Huang <sup>1</sup>, Xindi Xu <sup>1</sup>, Tianyu Li <sup>1</sup> and Hui Tian <sup>1</sup>

<sup>1</sup> Department of Chemistry and Chemical Engineering, Kunming University, Kunming 650214, Yunnan, China; ljj332195924@hotmail.com (J.-C.X.); sjr15887410670@hotmail.com (J.-R.S.); hmf668648@hotmail.com (M.-F.H.); xu1768644060@sohu.com (X.X.); ltyyt1999@sina.com (T.L.); thnb666@sina.com (H.T.)

<sup>2</sup> Yunnan Provincial Research Center for Plastic Films Engineering Technology, Kunming 650214, Yunnan, China

<sup>3</sup> High School Affiliated to Minzu University of China Kunming Wuhua Experimental School, 6# Chenjiaying Road, Wuhua District, Kunming 650102, Yunnan, China; liuting1124966147@hotmail.com

\* Correspondence: wuqiongkm@163.com

Received: 30 March 2020; Accepted: 15 April 2020; Published: 23 April 2020



**Abstract:** To identify the effects of halogen bonding in the architecture of Schiff base complex supramolecular networks, we introduced halogenated Schiff-base *3-Br-5-Cl-salen* as ligand and isolated a new salen-type manganese(III) complex  $[\text{Mn}^{\text{III}}(\text{Cl})(\text{H}_2\text{O})(3\text{-Br-5-Cl-salen})]$  (**1**) where *3-Br-5-Cl-salen* = *N,N'*-bis(3-bromo-5-chlorosalicylidene)-1,2-diamine. The complex was investigated in the solid-state for halogen bonds (XBs) by single crystal X-ray structure analysis. Meanwhile, theoretical calculations were carried out to rationalize the formation mechanism of different types of XBs in the complex. The analysis result of electronic structure of the halogen bonds indicated that the chlorine atom coordinated to the Mn(III) center possesses the most negative potential and acts as anionic XB acceptor (electron donor) to the adjacent substituted halogens on the ligand, meanwhile the intermolecular Mn-Cl...X-C halogen bonding plays a significant role in directing the packing arrangement of adjacent molecules and linking the 2D layers into a 3D network. In order to verify the above results and acquire detailed information, the title complex was further analyzed by using the Hirshfeld surface analyses.

**Keywords:** halogen bond; Schiff-base complex; DFT studies; charge distribution; Hirshfeld surfaces; supramolecular networks

## 1. Introduction

Engineering well-defined molecules into specific crystal network has been one of the frontiers in material science [1–3]. Although the strength and energy of non-covalent interactions are relatively small in comparison with those of covalent bond, large numbers of non-covalent interactions not only play important roles in the construction of crystal frameworks but also relate to various physicochemical properties, among which the most classic and widely studied intermolecular interaction is hydrogen bond [4–6]. Because of its high energy and directional character, the hydrogen bond is considered to be a structure-directing agent and, to some extent, can be used to construct specific molecular assemblies [7,8]. With the further development of research, however, because the constitution of hydrogen bond is relatively simple, in some cases it is difficult to achieve the goal of fine tuning the

architecture and the intermolecular forces of supramolecular materials [9]. Therefore, it has become an urgent subject to develop a substitution of hydrogen bonds in crystal engineering [10,11].

Recent years, with the progress made in terms of theoretical and experimental studies, researchers revealed the anisotropic charge density distribution nature of covalently bound halogens, by which a directional intermolecular interaction called halogen bond (X-bond or XB) generate between halogen and Lewis base (electron donation site) and arouse growing interest [12,13]. Not only is the strength of X-bond stronger than that of a wide range of other weak noncovalent contacts such as hydrophobic interactions, dipole–dipole bonds, and  $\pi$ – $\pi$  force, but the geometries of XB are more diverse [14–16]. Therefore, halogen bonding has been recognized as a promising alternative to hydrogen bonding in the self-assembly of a family of supramolecular architectures, especially in the fields of crystal engineering and material chemistry [15,17–19].

Initially, the studies on halogen bonds have been mainly focused on pure organic systems owing to the limited computational resources and ideal experimental models, few researchers have specially concern the electronic structure and topological properties of halogen bonds in metal complexes [20–24]. Recently, pioneer researches have looked at the methods for incorporating coordination polymers into X-bonded systems [25–27]. It was found that some ionic coordination complexes containing ionic inorganic ligands (e.g.,  $\text{Cl}^-$ ,  $\text{CN}^-$ ,  $\text{SCN}^-$  etc.) can be used as halogen bonding acceptors [28]. In some studies, metal complex cations can serve as charge-balanced objects in the framework of halogen bonds formed between halide anion and neutral X-bonded donor sites [10,29]. Whereas researches about other types of coordination polymers are still rather rare, Schiff base type complexes, as an important member of coordination family, have attracted much attention because of their unique structures and physicochemical properties [30,31]. Although the considerable progress that has been made in different frontier sciences, to the best of our knowledge, up to the present, still no work has specifically concerned the electronic configuration as well as the influence of halogen bonds on Schiff base complexes.

With the aim of exploring the electronic structure and topologies of X-bonded network of Schiff base complexes, we chose classic tetradentate salen-type Schiff base as ligands (3-Br-5Cl-salen = *N,N'*-bis(3-bromo-5-chlorosalicylidene)-diamine), and synthesized a new halogenate salen-type complex  $[\text{Mn}^{\text{III}}(3\text{-Br-5Cl-salen})(\text{Cl})(\text{H}_2\text{O})]$  (1). Theoretical analysis suggested that XBs play a key role in linking Schiff-base 2D layers into 3D frameworks.

## 2. Experimental

### 2.1. Material and Physical Measurements

All chemicals and solvents chosen for this work were purchased from the Aladdin Reagents (Shanghai) Co. Ltd. and were used without further purification. Elemental analyses were completed by using a Perkin-Elmer 240C instrument. PLASMA-SPEC (I) ICP atomic emission spectrometer was used to analyze the content of Mn (PerkinElmer, Shanghai, China).

### 2.2. Synthesis of the Complex

#### Synthesis of $[\text{Mn}^{\text{III}}(3\text{-Br-5Cl-salen})(\text{Cl})(\text{H}_2\text{O})]$ (1)

3-bromo-5-chlorosalicylaldehyd (0.160 g, 1.0 mmol) (Aladdin, Shanghai, China) and diamine (Aladdin, Shanghai, China) (0.03 g, 0.5 mmol) were dissolved in methanol (Aladdin, Shanghai, China) (30mL) under stirring and the resulting solution refluxed at 80 °C for 1 h. Then manganese chloride (0.197g) (Aladdin, Shanghai, China) was added in one portion to the solution under stirring at 60 °C for another 2 h. After the reaction was cooled down at room temperature, the brownish red filtrate was left to crystallize for one week in a beaker at room temperature. Brown crystals were filtered and dried in air.

### 2.3. X-Ray Crystal Structure Analysis

Single-crystal datasets were collected at 293(2) K on an automated diffractometer equipped with MoK $\alpha$  radiation ( $\lambda = 0.71073 \text{ \AA}$ ) and Cryostream cooler (Oxford Cryosystem). The title compound was investigated via polarizability using the CrysAlis<sup>Pro</sup> software according to the classic Lorentz equation [32]. Crystal structures of **1** were solved by direct methods and refined with full-matrix on  $F^2$  computations using the Olex2 software program [33]. In the final refinement, all the non-H atoms were anisotropically refined. All H atoms were refined using a riding model with C-H = 0.97  $\text{\AA}$  and  $U_{\text{iso}}(\text{H}) = 1.5 U_{\text{eq}}(\text{C})$  or  $1.2 U_{\text{eq}}(\text{C})$ , with aromatic C-H = 0.93  $\text{\AA}$ . Crystal data and details of structural determination and refinement for **1** are summarized in Table 1. Selected bond lengths and angles for **1** are collected in Table S1.

**Table 1.** Crystal data and details of structural determination and refinement for **1**.

Empirical Formula	C <sub>16</sub> H <sub>12</sub> Br <sub>3</sub> Cl <sub>3</sub> Mn <sub>1</sub> N <sub>2</sub> O <sub>3</sub>
<i>Mr</i>	601.37
Temperature/K	293(2)
Wavelength/ $\text{\AA}$	0.71073
Crystal system	Monoclinic
space group	<i>P</i> 21/ <i>c</i>
<i>a</i> / $\text{\AA}$	12.4164(12)
<i>b</i> / $\text{\AA}$	13.5291(18)
<i>c</i> / $\text{\AA}$	13.2867(9)
$\beta$ /deg	122.347(6)
Volume/ $\text{\AA}^3$	1142.6(3)
<i>Z</i>	4
Calculated density	1885.6(3) Mg/m <sup>3</sup>
Absorption coefficient	5.384 mm <sup>-1</sup>
F(000)	1168
Theta range for data collection	3.52 to 25.00 deg
Limiting indices	$-13 \leq h \leq 14, -15 \leq k \leq 16, -15 \leq l \leq 10$
Reflections collected/unique	4827/2812 [R(int) = 0.0513]
Completeness to theta = 25.00	99.7%
Refinement method	Full-matrix least-squares on $F^2$
Goodness-of-fit on $F^2$	0.962
Final R indices [ $I > 2\sigma(I)$ ]	$R_1 = 0.0619, wR_2 = 0.0978$
R indices (all data)	$R_1 = 0.0986, wR_2 = 0.1098$

Spartan 14 V1.1.4 Wave function molecular modeling suite was used for the calculations of compound **1** on a personal computer by means of DFT method [34]. Hirshfeld surfaces analyses were carried out using CrystalExplorer 17.5 software [35] and the TONTO system [36].

Crystallographic data (excluding structure factors) for the structure in this paper have been deposited with the Cambridge Crystallographic Data Centre, CCDC, 12 Union Road, Cambridge CB21EZ, UK. Copies of the data can be obtained free of charge on quoting the depository number CCDC-1958103 (Fax: +44-1223-336-033; E-Mail: deposit@ccdc.cam.ac.uk, <http://www.ccdc.cam.ac.uk>) [37].

The complex crystallizes in monoclinic space group *P*21/*c*. There is one manganese(III) center, one 3-*Br*-5*Cl*-salen salen-type ligand, one chloride anion, and one water molecule in the asymmetric unit (see Figure 1a). The basal plane of Mn<sup>III</sup> center of **1** is chelated by two oxygen and two nitrogen atoms from 3-*Br*-5*Cl*-salen unit, with Mn-O(N) bond distances ranging from 1.864(5) to 2.027(5)  $\text{\AA}$ , and O(N)-Mn-O bond angles of 80.8(2) to 173.0(2). The length of Mn-N is, on average, 2.1395(5)  $\text{\AA}$  longer than that of Mn-O [1.898(6)  $\text{\AA}$ ]. The dihedral angle between two benzene rings is 8.38(58)°. Thus, the molecule exhibits an overall coplanar architecture, which is, as can be clearly observed, in accordance with those reported in non-halogenated Schiff base complexes [38,39].

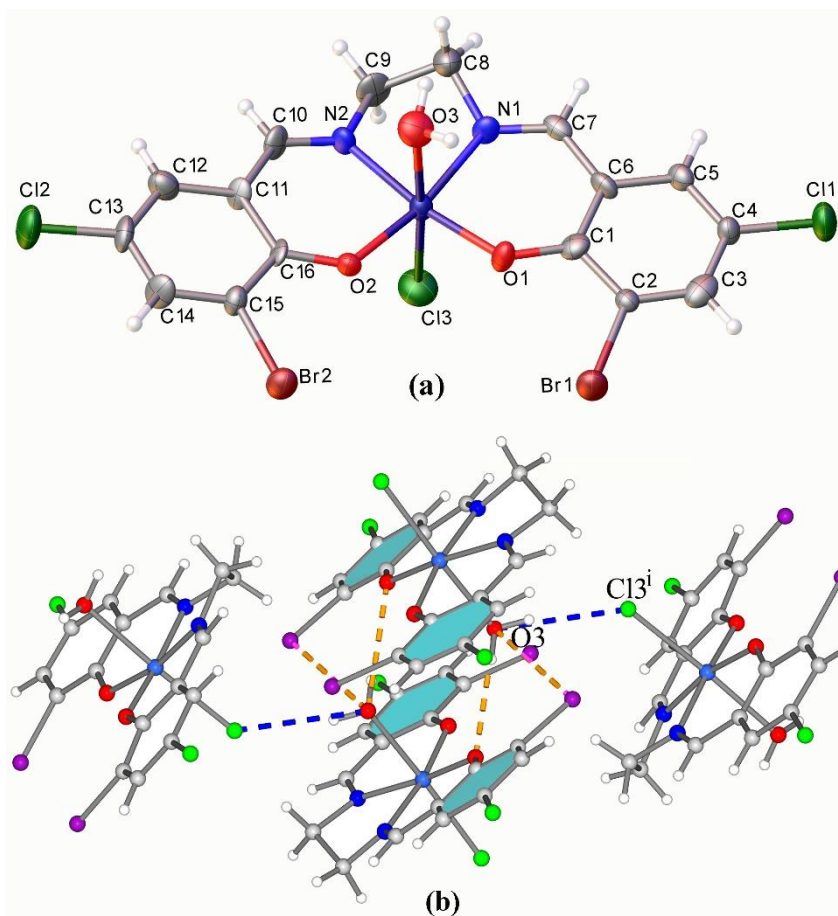


**Figure 1.** (a) The molecular structures of compound **1**, showing the atomic displacement parameters at 50% probability. (b) Ball-and-stick representation of H-bonded supramolecular dimer network of compound **1**.

The apical positions of **1** are occupied by one oxygen atom O(3) from a water molecule and one chlorine ligand Cl(3). From which we can clearly see that owing to the Jahn-Teller effect of high-spin  $d^4$  metal center, the hexa-coordinate  $Mn^{III}$  center possesses an elongated axis, furnishing a distorted octahedral geometry. The bond lengths of Mn(1)–O(3) and Mn(1)–Cl(3) are 2.301(6) and 2.500(3) Å, respectively, much longer than those of the basal plane.

It is revealed by PLATON software that a self-assembled supramolecular dimer is built up of two adjacent monomers which are linked by  $\pi$ – $\pi$ , O–H...O and O–H...Br intermolecular hydrogen interactions (see Figure 1b and Figure S1 (Supplementary Materials)) [40]. Then, the coordination oxygen atoms O(3) form intermolecular hydrogen bonds with the adjacent coordinated chlorine atom Cl(3)<sup>i</sup> [i: 1–x, 0.5+y, 1.5–z] which links the neighboring self-assembled supramolecular dimers to form a one-dimensional chain structure (Figures 1b and 2a). In the bc plane, the 1D chains were further linked together through the O–H...Cl H-bonds (O(3)–H(3A)...Cl(3)<sup>iii</sup> [iii: 1–x, –0.5+y, 1.5–z]) to form supramolecular dimer 2D layers. Details of intermolecular hydrogen bonding interactions are given in Table 2.

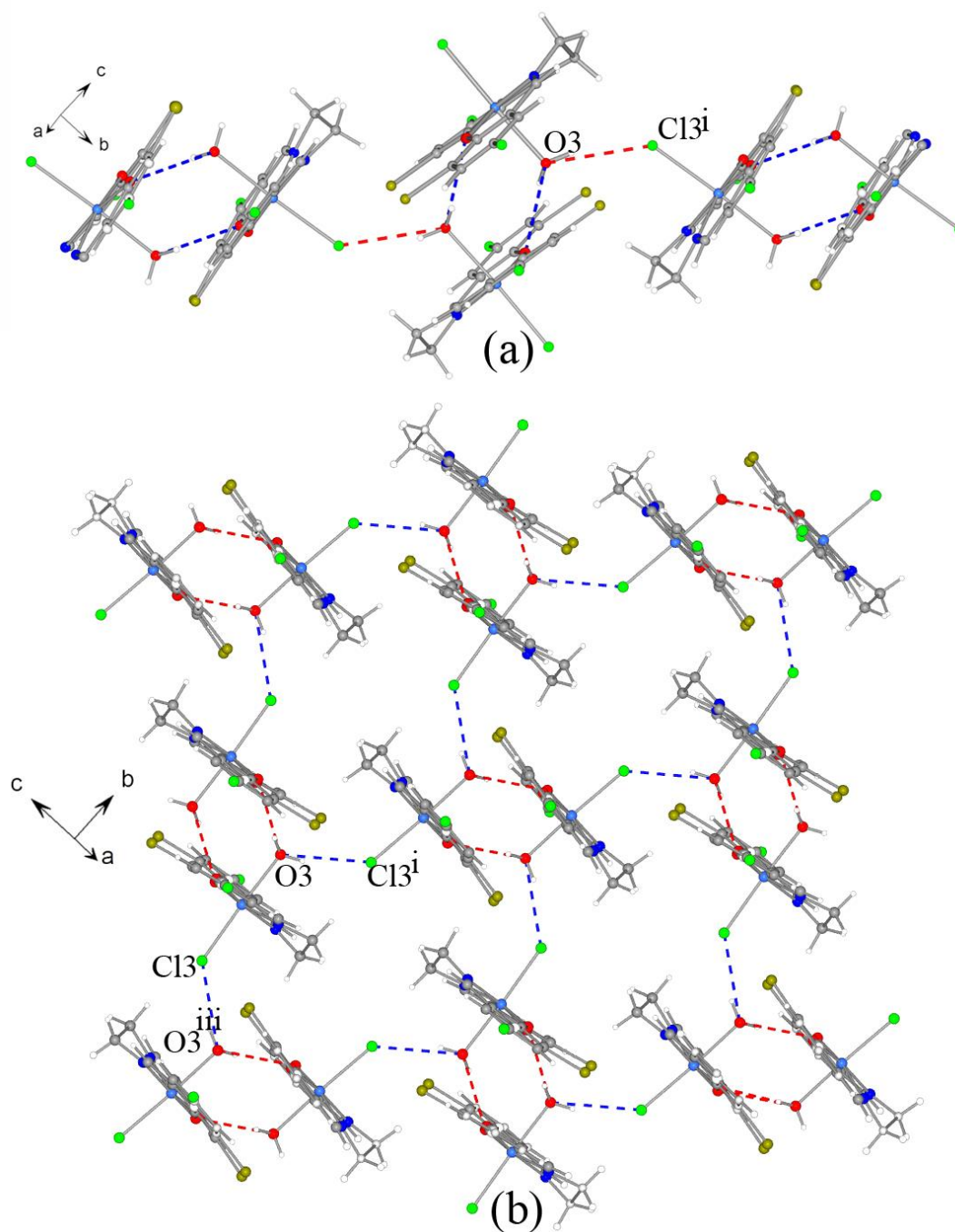


**Figure 2.** The crystal packing of complex 1 showing (a) intermolecular hydrogen bonding which is responsible for the stable packing of the chains; (b) intermolecular hydrogen bonding for a 3D framework. Color: the intermolecular O–H...O hydrogen bonds are shown as red dashed lines; the intermolecular O–H...Cl hydrogen bonds are shown as blue dashed lines.

**Table 2.** Hydrogen bonding geometry.

D–H...A	D–H, Å	H...A, Å	D...A, Å	D–H...A, deg
O(3)–H(3A)...Cl(3) <sup>i</sup>	0.85	2.52	3.303(8)	154
O(3)–H(3B)...Br(2) <sup>ii</sup>	0.85	2.84	3.381(9)	123
O(3)–H(3B)...O(2) <sup>ii</sup>	0.85	2.4	3.216(9)	161

Symmetry codes: (i) 1-x,-y,-z; (ii) 1-x,-1/2+y,1/2-z.

It is well-known that PLATON software is effective in qualitative analyses of classic intermolecular contacts. However, the information it can give about non-classical weak contacts and quantitative results is very limited. Platon only shows the 1D to 2D intermolecular contacts, this seems to suggest that Van der Waals forces play a dominating role in the organization of the 2D layer into 3D network. However, further theoretical calculation shows that there is a close relationship between XB and 3D crystal structure. Detailed structural discussion will be presented in the theoretical analysis section.

#### 2.4. Optimized Structure and HOMO-LUMO

It is known that the electronic properties and reactivity of complex can be elucidated by the analysis of the frontier molecular orbitals [41]. The fit view of experimental and optimized structures of the title compound is given in Figure 3 and Figure S2 (Supplementary Materials). The bond distances and angles of the optimized molecular structure are basically consistent with the experimental structure; generally slight differences are observed because the optimized geometry was obtained by gas-phase DFT optimizations [42]. Selected frontier molecular orbitals three-dimensional plots of 1 are given in Figure 4. The HOMO surface is mainly localized around benzene rings and the coordination chlorine atom, and the LUMO around the metal centers and -C=N- double bond showing an effective communication from  $\pi$ -orbitals throughout the ligand.

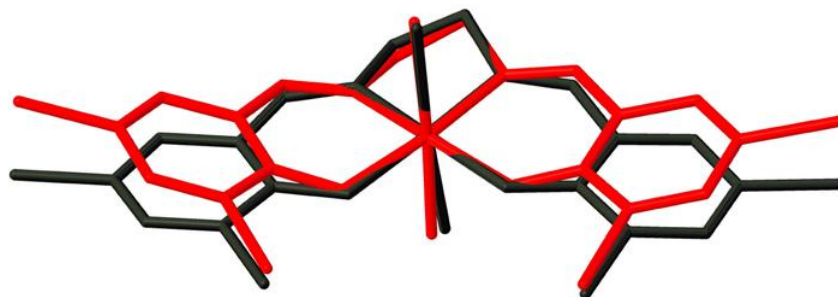


**Figure 3.** The overlay view of experimental structure and optimized structures of 1 are given in black and red, respectively. Hydrogen atoms have been omitted for clarity.

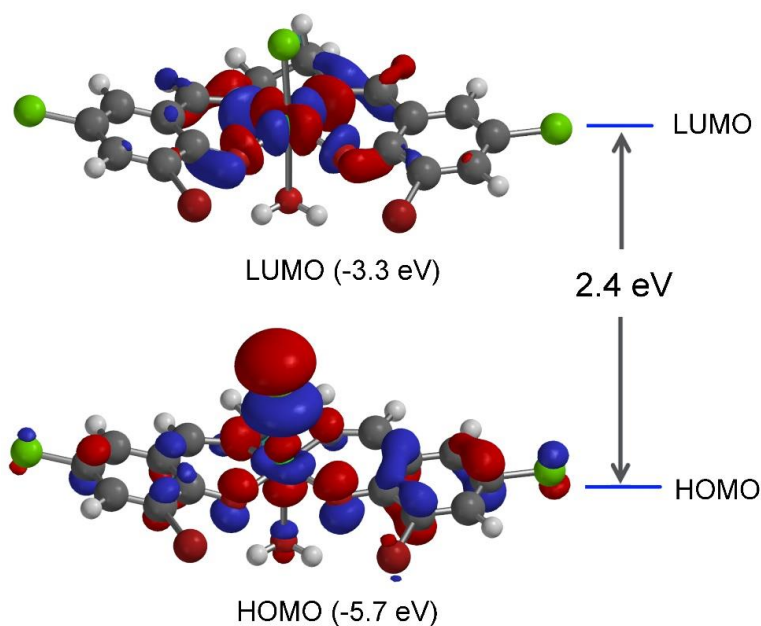


**Figure 4.** Visual representation of molecular orbital surfaces for compound 1.

In order to evaluate the weak contacts and electrochemical reactivity of the title complex, ESP and MEP maps were created by using the B3LYP/6-311G level in ground state [43]. The region shown as

convex surface that represents negative electrostatic potential, which wholly covers around the chlorine ligand (Cl(3)) (see Figure 5a), mostly covers phenoxy oxygen atoms (O(1) and O(2)), and partially covers bromine atoms (Br(1) and Br(2)) in a small semicircle region near the benzene ring, indicating the most highly negative sites are localized around the atoms. Noteworthy, compared with bromine atoms, the substitute chlorine atoms (Cl(1) and Cl(2)) on the benzene rings do not display a higher negative potential, similar results can be found in the molecular electrostatic potential (MEP) map.

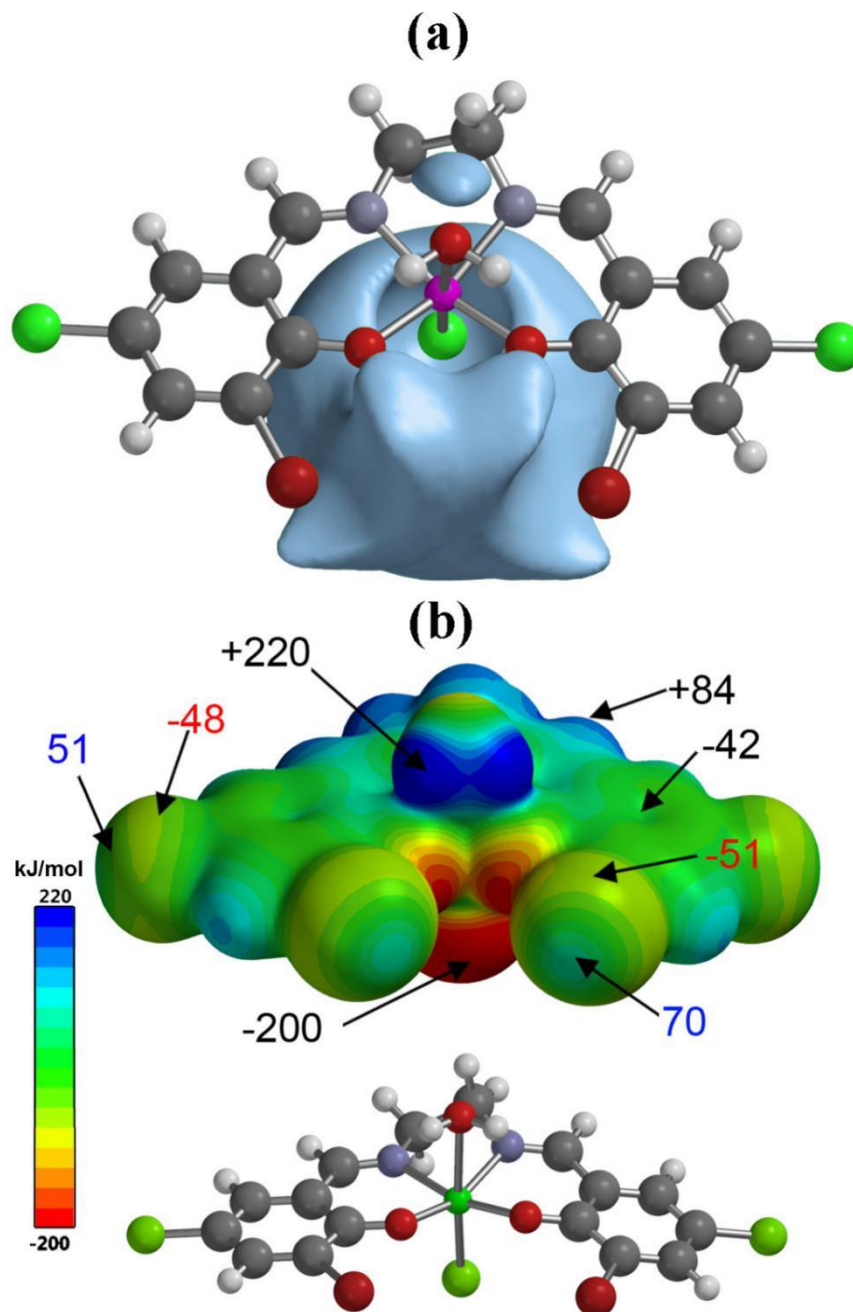


**Figure 5.** Molecular surface plot of the title compound: (a) electrostatic potential surface and (b) molecular electrostatic potential (MEP) surface of compound 1. The MEP values at selected points are given in  $\text{kJ/mol}^{-1}$ .

The MEP for the title compound is scaled from  $-200 \text{ kJ mol}^{-1}$  to  $+220 \text{ kJ mol}^{-1}$ , and the quantitative molecular electrostatic potential surface is displayed with color: red indicates the negative regions and

blue indicates the positive regions. As is shown in Figure 5b and Figure S3 (Supplementary Materials), the region around the halogen atom (Cl(3)) that coordinated to the Mn(III) center ( $-200 \text{ kJ}\cdot\text{mol}^{-1}$ ) exhibits the most highly negative electrostatic potential. Meanwhile, this region is also influenced by the phenoxo oxygen atom ( $-158 \text{ kJ}\cdot\text{mol}^{-1}$ ). Consequently, we can predict that the atom in the region acts as an electron donor in intermolecular interactions. The region of hydrogen atoms on the coordination water molecule ( $220 \text{ kJ}\cdot\text{mol}^{-1}$ ) and the amine group at the molecular plane ( $84 \text{ kJ}\cdot\text{mol}^{-1}$ ) exhibits the most highly positive electrostatic potential. Further study indicated that the bromine and chlorine atoms on the benzene rings present quite different values in different directions. More specifically, along the C-X bond axis, the MEP potential is positive, the MEP values for Br(1) and Cl(2) are calculated to be  $70 \text{ kJ}\cdot\text{mol}^{-1}$  and  $51 \text{ kJ}\cdot\text{mol}^{-1}$ , respectively; whereas the potentials in the direction perpendicular to the axis are negative, that for Br(1) and Cl(2) to be  $-51 \text{ kJ}\cdot\text{mol}^{-1}$  and  $-48 \text{ kJ}\cdot\text{mol}^{-1}$ , respectively. That is to say along C-X bond direction halogens is electrophilic ( $\delta^+$ ) which can act as  $\sigma$ -hole to interact with negatively charged electrostatic nucleophile Figure 6. In addition, although Br atom is close to the most negative region(chlorine ligand and phenoxo oxygen atoms) of the whole molecule, the positive potential of Br along C-Br bond direction is still higher than that in the C-Cl direction of Cl atom. These observation show that the electrostatic potential distribution of halogen atoms on the salen type ligand is basically consistent with other types of halogenated organic compounds.

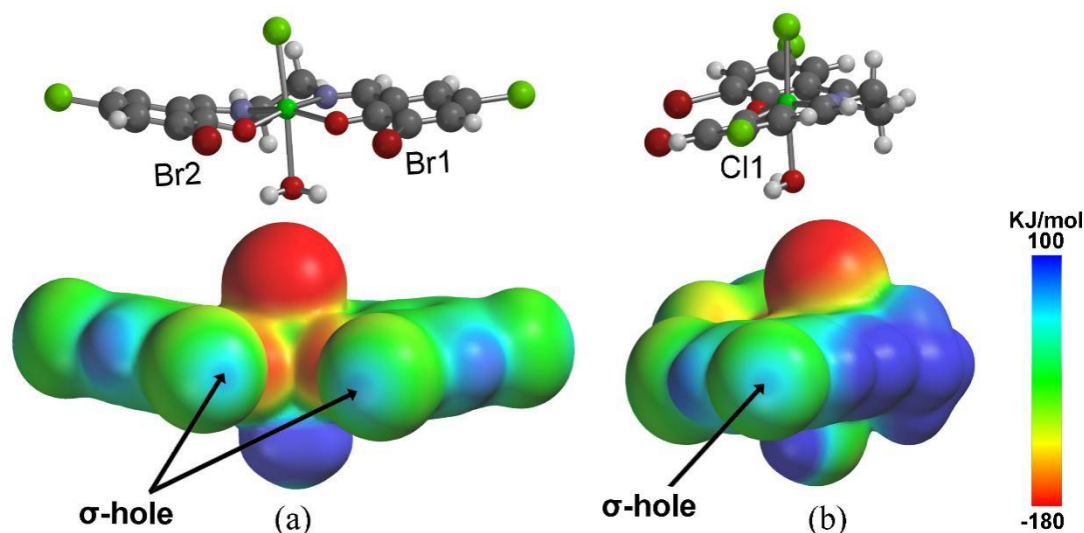


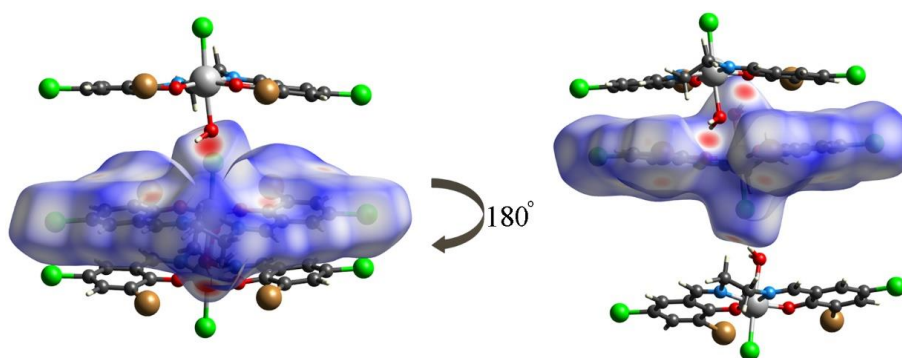
**Figure 6.** Molecular electrostatic potential calculations of 1, (a)  $\sigma$ -hole of bromine atoms (b)  $\sigma$ -hole of chlorine atom. Color range (kJ/mol): where red stands for lower than  $-140$ ; yellow between  $-140$  and  $100$ ; green between  $-30$  and  $30$ ; and blue greater than  $50$ .

### 2.5. Hirshfeld Surface Analysis

Hirshfeld surface analysis provides insights into the detailed information about the strength of intermolecular interactions. A better understanding of the issue can contribute to addressing the challenge of quantitatively understanding the intermolecular contacts using visual information of color and shades on the surfaces [35]. Therefore, in this work, Hirshfeld surface analysis was used to analyze the intermolecular interactions in the crystal packing. Moreover, visualized images of the molecular structure and the positioning of Hirshfeld surfaces were also employed to elucidate the interaction of specific atoms and orientations.

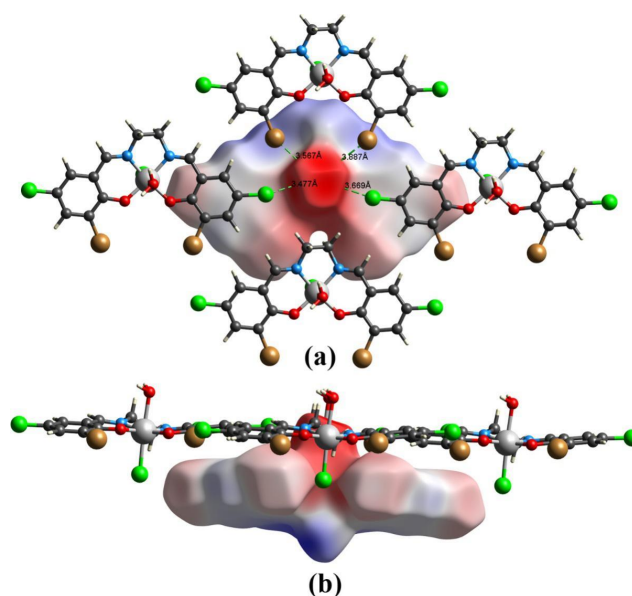
The interactions with normalized contact distance in crystal structure shorter than the sum of the corresponding van der Waals radii of the atoms, are highlighted by red spots and mapped with negative  $d_{norm}$  value on the Hirshfeld surface, whereas the contacts around that of van der Waals radii with zero  $d_{norm}$  value are plotted in white color, and the longer contacts with the positive  $d_{norm}$  value are represented in blue color (Figure S4 (Supplementary Materials)) [44]. The largest red region in

Figure 7(left) is originated from strong hydrogen bonding contacts within the coordination chlorine atom and adjacent oxygen atom (O–H...Cl H-bond (O(3)–H(3A)...Cl(3)<sup>iii</sup> [iii: 1-x, -0.5+y, 1.5-z] [i: -0.5-y, 0.5+z]). This plot is in accordance with electrostatic potential surfaces calculation result that the most strong interaction occurs between the most negative and the most positive region of the title compound. Secondary obvious red regions Figure 7(right) appears at the other side of **1**, which are ascribed to a pair of symmetric hydrogen bonds within the self-assembled supramolecular dimer: O(3)–H(3A)...O(3)<sup>i</sup> and O(3)...O(3)<sup>i</sup>–H(3A)<sup>i</sup>.



**Figure 7.** O–H...Cl interaction in **1** wherein the Hirshfeld surface emphasizes short intermolecular contacts.

Herein we carried out the mapping of the electrostatic potential on Hirshfeld surfaces at the B3LYP/3-21G level of theory (see Figure 8) [45]. It is clearly shown that the chlorine ligands act as halogen bonding acceptors and link three adjacent molecules participating in the formation of halogen bonding. Although these molecules are arranged in different directions, all the C–X...Cl–Mn angles are close to 180° (Figure 8a, Figure S5 and Table S2 (Supplementary Materials)). Therefore, it is concluded that this is due to the key role of XBs that leads to the organization of the 2D layered sheets of **1** (Figure 8b). Furthermore, structural analyses show that 2D layered structures are bound to form a 3D supramolecular framework via multiply halogen bonding (Figure 9).



**Figure 8.** The three-dimensional map of the potential across the plane for quantifying the intermolecular interactions within the crystal structure. (a) C–X...Cl–Mn interactions between adjacent molecules; (b) XB induced layered structure.

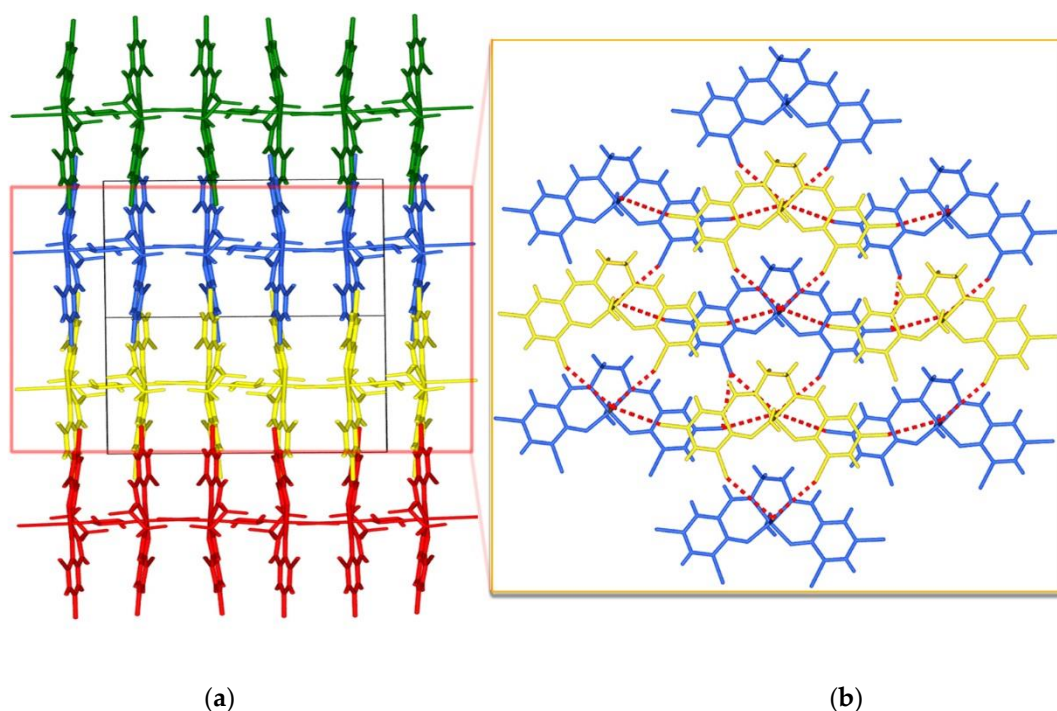


**Figure 9.** The packing configurations of **1** (a) 3-dimensional network (b) 3-dimensional structure constructed by means of the aggregation behavior fueled by hydrogen bonding. Color code: red dashed lines represent the intermolecular C-X...Cl-Mn hydrogen bonds.

### 2.6. Intermolecular Interaction Energy

In this work, we used the CrystalExplorer software to calculate and display the interaction energy in a molecular crystal by using the B3LYP method with 3–21G basis set level [46]. Analyzing and quantifying intermolecular interactions in a crystal lattice, including repulsion, electrostatic, dispersion, and polarization etc., could help researchers gain an insight into the underlying interaction energy that happens and leads to the organization of crystal packing into supramolecular architectures in crystalline materials [47].

The molecular environment of the title structure was built at its center and around with a maximum distance of 3.8 Å. The energies' benchmark was calculated according to Mackenzie's method to scale different energy frameworks, which shows that the scale factors for electrostatic, dispersion, polarization, and repulsion are 1.057, 0.740, 0.871, and 0.618, respectively.

The relative strengths in interaction energy of molecular packing in all directions obtained here exhibit cylinder-shaped energy frameworks (see Figure 10). Some insignificant contacts weaker than the threshold energy value of 10 kcal/mol have been omitted from the original calculation for clarity. From the perspective of the computational results of the interaction energies, it is also revealed that XB interaction should be of fundamental importance because of the fact that XBs conducting electrostatic interactions (−224.4 kJ/mol) play a dominant role in the crystal structure of the investigated system. Additionally, the polarization, repulsion, and total interaction energies are found to be −89.6 kJ/mol, 275.5 kJ/mol, −326.9 kJ/mol, respectively. Details of the interaction energy calculation for **1** are presented in Table S1.

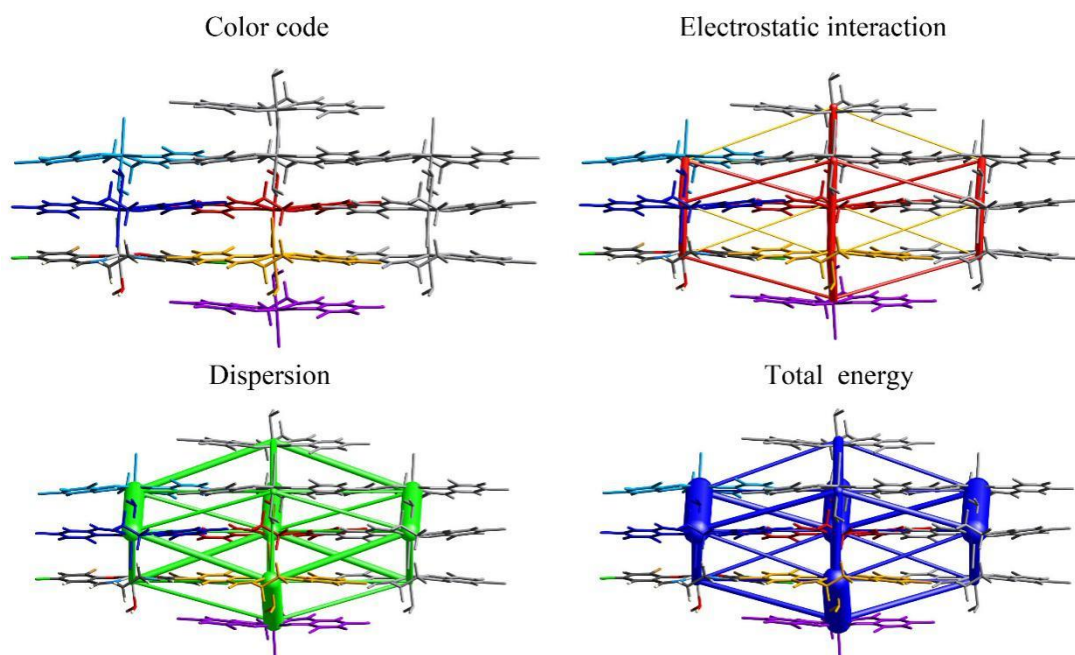


**Figure 10.** Visualization of the intermolecular interaction energy: red for Coulomb, green for dispersion, and blue for total interaction energies of the title structure along a axis.

### 3. Conclusions

In order to get insights of the electronic structure and topologies of XBs in Schiff base complexes, a new hetero-halogenated Schiff-base complex was synthesized and determined by single crystal X-ray diffraction. Crystal structure analyses revealed that classic H-bond is the main driving force in linking the molecules into 1D and 2D structures, and no significant interactions are found from 2D layers to 3D network. Whereas, theoretical calculation gives us a further information about the energy architecture of the 3D structure of this halogenated compound.

Theoretical calculations indicated that the chlorine ligands have the most negative potential, which acts as anion XB acceptors to the adjacent halogens to form multiple XBs. This kind of interaction not only directs the adjacent molecules to form a 2D layered structure but also links the 2D layers into a 3D framework. The intermolecular interaction energy was also evaluated by Hirshfeld surface analysis, and the results indicate that the XB conducting electrostatic interactions are predominant over the crystal packing. Because the strength of XBs could be mediated by different halogen atoms, we could regulate the expansion of 2D layers into 3D frameworks by changing the halogen atoms and/or coordinated ones to form different XBs with different strength.

**Supplementary Materials:** The following are available online at <http://www.mdpi.com/2073-4352/10/4/334/s1>. Figure S1: The self-assembled supramolecular dimer of 1. Figure S2: The optimized structures. Figure S3: Full molecular ESP. Figure S4: Hirshfeld surfaces map. Figure S5: short contact of 1. Table S1: Table S1. Molecular pair wise interaction energies (kJ/mol) obtained from the energy framework calculation for compound 1. Table S2. Selected X-Bond Distances and Angles.

**Author Contributions:** Methodology, Q.W., J.-R.S., X.X., H.T., and M.-F.H.; investigation, Q.W., and J.-C.X.; resources J.-R.S.; software, conceptualization Q.W. and T.L.; formal analysis, X.X. and J.-R.S.; validation, J.-C.X. and C.Z.; supervision, Q.W.; writing—original draft preparation, J.-C.X., C.Z.; project administration, Q.W.; visualization, Q.W. and J.-C.X.; writing—review and editing, J.-C.X.; funding acquisition, Q.W. These authors contribute equally to this work. All authors have read and agree to the published version of the manuscript.

**Funding:** This research has been funded by the National Nature Science Foundation of China, grant number 31760257; the Joint Basic Research Program (partial) of Yunnan Provincial Undergraduate Universities, grant number 2017FH001-002 and the Recruitment Program of Yunnan Province Experts Provincial Young Talents, grant number 2019HB098.

**Acknowledgments:** The authors thank the National Nature Science Foundation of China (No. 31760257) as well as the Joint Basic Research Program (partial) of Yunnan Provincial Undergraduate Universities (2017FH001–002) and the Recruitment Program of Yunnan Province Experts Provincial Young Talents (2019HB098) for financial support.

**Conflicts of Interest:** The authors declare no conflict of interest. The funders had no role in the design of the study; in the collection, analyses, or interpretation of data; in the writing of the manuscript, or in the decision to publish the results.

## References

1. Voorhaar, L.; Hoogenboom, R. Supramolecular polymer networks: Hydrogels and bulk materials. *Chem. Soc. Rev.* **2016**, *45*, 4013–4031. [[CrossRef](#)]
2. Okesola, B.O.; Smith, D.K. Applying low-molecular weight supramolecular gelators in an environmental setting-self-assembled gels as smart materials for pollutant removal. *Chem. Soc. Rev.* **2016**, *45*, 4226–4251. [[CrossRef](#)]
3. Pang, H.; Peng, J.; Sha, J.; Tian, A.; Zhang, P.; Chen, Y.; Zhu, M. A molecular crown analogue templated by Keggin polyanions: Synthesis, structure, and electrochemical and luminescent properties. *Z. Nat. B* **2015**, *70*, 547–553.
4. Xia, Q.; Yuan, C.; Li, Y.; Cui, Y. Design and assembly of a chiral composite metal-organic framework for efficient asymmetric sequential transformation of alkenes to amino alcohols. *Chem. Commun.* **2019**, *55*, 9136–9139. [[CrossRef](#)]
5. Kirillov, A.M. Hexamethylenetetramine: An old new building block for design of coordination polymers. *Coord. Chem. Rev.* **2011**, *255*, 1603–1622. [[CrossRef](#)]
6. Zhang, D.S.; Zhang, Y.Z.; Gao, J.; Liu, H.L.; Hu, H.; Geng, L.L.; Zhang, X.; Li, Y.W. Structure modulation from unstable to stable MOFs by regulating secondary N-donor ligands. *Dalton Trans.* **2018**, *47*, 14025–14032. [[CrossRef](#)] [[PubMed](#)]
7. Martins, G.A.V.; Gieck, C.; Coluccia, S.; Marchese, L.; Pastore, H.O. One Step Further in Understanding the Role of Hydrogen Bonds in Directing the Synthesis of CHA Analogue Molecular Sieves. *J. Phys. Chem. C* **2009**, *113*, 10675–10680. [[CrossRef](#)]
8. Ong, W.-J.; Tan, L.-L.; Chai, S.-P.; Yong, S.-T. Graphene oxide as a structure-directing agent for the two-dimensional interface engineering of sandwich-like graphene-g-C<sub>3</sub>N<sub>4</sub> hybrid nanostructures with enhanced visible-light photoreduction of CO<sub>2</sub> to methane. *Chem. Commun.* **2015**, *51*, 858–861. [[CrossRef](#)] [[PubMed](#)]
9. Thota, B.N.S.; Urner, L.H.; Haag, R. Supramolecular Architectures of Dendritic Amphiphiles in Water. *Chem. Rev.* **2016**, *116*, 2079–2102. [[CrossRef](#)]
10. Gilday, L.C.; Robinson, S.W.; Barendt, T.A.; Langton, M.J.; Mullaney, B.R.; Beer, P.D. Halogen Bonding in Supramolecular Chemistry. *Chem. Rev.* **2015**, *115*, 7118–7195. [[CrossRef](#)]
11. Metrangolo, P.; Resnati, G. Halogen Bonding: Where We Are and Where We Are Going. *Cryst. Growth Des.* **2012**, *12*, 5835–5838. [[CrossRef](#)]
12. Cavallo, G.; Metrangolo, P.; Milani, R.; Pilati, T.; Terraneo, G. The Halogen Bond. *Chem. Rev.* **2016**, *116*, 2478–2601. [[CrossRef](#)] [[PubMed](#)]
13. Huber, S.M.; Scanlon, J.D.; Jimenez-Izal, E.; Ugalde, J.M.; Infante, I. On the directionality of halogen bonding. *Phys. Chem. Chem. Phys.* **2013**, *15*, 10350–10357. [[CrossRef](#)] [[PubMed](#)]
14. Gaspard, D.; Seddon, K.R.; Robertson, P.K.J.; Gunaratne, H.Q.N. Halogen-bond mediated efficient storage of extremely volatile perfluoroiodides in ionic liquids. *Chem. Commun.* **2019**, *55*, 9088–9091. [[CrossRef](#)] [[PubMed](#)]
15. Varadwaj, P.R.; Varadwaj, A.; Marques, H.M. Halogen Bonding: A Halogen-Centered Noncovalent Interaction Yet to Be Understood. *Inorganics* **2019**, *7*, 40. [[CrossRef](#)]
16. Buntara Sanjeeva, K.; Pigliacelli, C.; Gazzera, L.; Dichiarante, V.; Baldelli Bombelli, F.; Metrangolo, P. Halogen bond-assisted self-assembly of gold nanoparticles in solution and on a planar surface. *Nanoscale* **2019**, *11*, 18407–18415. [[CrossRef](#)] [[PubMed](#)]
17. Scheiner, S. On the capability of metal-halogen groups to participate in halogen bonds. *CrystEngComm* **2019**, *21*, 2875–2883. [[CrossRef](#)]
18. Mirocki, A.; Sikorski, A. Influence of Halogen Substituent on the Self-Assembly and Crystal Packing of Multicomponent Crystals Formed from Ethacridine and Meta-Halobenzoic Acids. *Crystals* **2020**, *10*, 79. [[CrossRef](#)]
19. Priimagi, A.; Cavallo, G.; Metrangolo, P.; Resnati, G. The Halogen Bond in the Design of Functional Supramolecular Materials: Recent Advances. *Acc. Chem. Res.* **2013**, *46*, 2686–2695. [[CrossRef](#)]

20. Pfrunder, M.C.; Micallef, A.S.; Rintoul, L.; Arnold, D.P.; McMurtrie, J. Interplay between the Supramolecular Motifs of Polypyridyl Metal Complexes and Halogen Bond Networks in Cocrystals. *Cryst. Growth Des.* **2016**, *16*, 681–695. [CrossRef]
21. Aakeröy, C.B.; Wijethunga, T.K.; Desper, J.; Đaković, M. Crystal Engineering with Iodoethynylnitrobenzenes: A Group of Highly Effective Halogen-Bond Donors. *Cryst. Growth Des.* **2015**, *15*, 3853–3861. [CrossRef]
22. Aakeröy, C.B.; Wijethunga, T.K.; Desper, J.; Đaković, M. Electrostatic Potential Differences and Halogen-Bond Selectivity. *Cryst. Growth Des.* **2016**, *16*, 2662–2670. [CrossRef]
23. Liu, R.; Wang, H.; Jin, W.J. Soft-Cavity-type Host–Guest Structure of Cocrystals with Good Luminescence Behavior Assembled by Halogen Bond and Other Weak Interactions. *Cryst. Growth Des.* **2017**, *17*, 3331–3337. [CrossRef]
24. Dumele, O.; Wu, D.; Trapp, N.; Goroff, N.; Diederich, F. Halogen Bonding of (Iodoethynyl)benzene Derivatives in Solution. *Org. Lett.* **2014**, *16*, 4722–4725. [CrossRef]
25. Awwadi, F.F.; Willett, R.D.; Twamley, B.; Turnbull, M.M.; Landee, C.P. Dual Behavior of Bromine Atoms in Supramolecular Chemistry: The Crystal Structure and Magnetic Properties of Two Copper(II) Coordination Polymers. *Cryst. Growth Des.* **2015**, *15*, 3746–3754. [CrossRef]
26. Lisac, K.; Cinčić, D. Simple design for metal-based halogen-bonded cocrystals utilizing the M–Cl···I motif. *CrystEngComm* **2018**, *20*, 5955–5963. [CrossRef]
27. Ding, X.; Tuikka, M.; Rissanen, K.; Haukka, M. Extended Assemblies of Ru(bpy)(CO)<sub>2</sub>X<sub>2</sub> (X = Cl, Br, I) Molecules Linked by 1,4-Diiodotetrafluoro-Benzene (DITFB) Halogen Bond Donors. *Crystals* **2019**, *9*, 319. [CrossRef]
28. Awwadi, F.F.; Turnbull, M.M.; Alwahsh, M.I.; Haddad, S.F. May halogen bonding interactions compete with Cu···Cl semi-coordinate bonds? Structural, magnetic and theoretical studies of two polymorphs of trans-bis(5-bromo-2-chloro pyridine)dichlorocopper(ii) and trans-bis(2,5-dichloropyridine)dichlorocopper(ii). *New J. Chem.* **2018**, *42*, 10642–10650. [CrossRef]
29. Stilinović, V.; Grgurić, T.; Piteša, T.; Nemeč, V.; Cinčić, D. Bifurcated and Monocentric Halogen Bonds in Cocrystals of Metal(II) Acetylacetonates with p-Dihalotetrafluorobenzenes. *Cryst. Growth Des.* **2019**, *19*, 1245–1256. [CrossRef]
30. Li, Y.; Wu, Q.; Lecren, L.; Clérac, R. Synthesis, structure and magnetism of new polynuclear transition metal aggregates assembled with Schiff-base ligand and anionic N-donor ligands. *J. Mol. Struct.* **2008**, *890*, 339–345. [CrossRef]
31. Senapati, T.; Pichon, C.; Ababei, R.; Mathonière, C.; Clérac, R. Cyanido-bridged Fe(III)-Mn(III) heterobimetallic materials built from Mn(III) Schiff base complexes and di- or tri-cyanido Fe(III) precursors. *Inorg. Chem.* **2012**, *51*, 3796–3812. [CrossRef] [PubMed]
32. *Agilent Technologies: CrysAlis<sup>PRO</sup> Software system, v.*; Agilent Technologies UK Ltd.: Oxford, UK, 2015.
33. Dolomanov, O.V.; Bourhis, L.J.; Gildea, R.J.; Howard, J.A.K.; Puschmann, H. OLEX2: A complete structure solution, refinement and analysis program. *J. Appl. Crystallogr.* **2010**, *42*, 339–341. [CrossRef]
34. *Spartan 14*; Wavefunction Inc.: Irvine, CA, USA, 2014.
35. Spackman, M.A.; Jayatilaka, D. Hirshfeld surface analysis. *CrystEngComm*. **2009**, *11*, 19–32. [CrossRef]
36. Jayatilaka, D.; Grimwood, D.J. Tonto: A Fortran Based Object-Oriented System for Quantum Chemistry and Crystallography. In Proceedings of the Computational Science—ICCS 2003, Berlin/Heidelberg, Germany, 2–4 June 2003; Sloop, P.M.A., Abramson, D., Bogdanov, A.V., Gorbachev, Y.E., Dongarra, J.J., Zomaya, A.Y., Eds.; Springer: Berlin/Heidelberg, Germany, 2003; pp. 142–151.
37. Available online: [www.ccdc.cam.ac.uk/data\\_request/cif](http://www.ccdc.cam.ac.uk/data_request/cif) (accessed on 8 October 2019).
38. Martinez, D.; Motevalli, M.; Watkinson, M. Aquachloro[N,N'-ethylenebis(salicylideneiminato)]manganese(III). *Acta Crystallogr. Sect. C* **2002**, *58*, m258–m260. [CrossRef] [PubMed]
39. Wu, Q.; Shi, Q.; Li, Y.-G.; Wang, E.B. Synthesis, crystal structure and magnetic properties of new Mn<sup>III</sup>–Cu<sup>II</sup> heterometallic aggregates based on multidentate Schiff-base ligands. *J. Coord. Chem.* **2008**, *61*, 3080–3091. [CrossRef]
40. Spek, A.L.J.; Spek, A.L. Single-crystal structure validation with the program PLATON. *J. Appl. Crystallogr.* **2003**, *36*, 7–13. [CrossRef]
41. Zhan, C.G.; Nichols, J.A.; Dixon, D.A. Ionization potential, electron affinity, electronegativity, hardness, and electron excitation energy: Molecular properties from density functional theory orbital energies. *J. Phys. Chem. A* **2003**, *107*, 4184–4195. [CrossRef]
42. Tepper, R.; Schubert, U.S. Halogen Bonding in Solution: Anion Recognition, Templated Self-Assembly, and Organocatalysis. *Angew. Chem. Int. Ed.* **2018**, *57*, 6004–6016. [CrossRef]
43. Andersson, M.P.; Uvdal, P. New Scale Factors for Harmonic Vibrational Frequencies Using the B3LYP Density Functional Method with the Triple- $\zeta$  Basis Set 6–311+G(d,p). *J. Phys. Chem. A* **2005**, *109*, 2937–2941. [CrossRef]

44. Demircioğlu, Z.; Özdemir, F.A.; Dayan, O.; Şerbetçi, Z.; Özdemir, N. Synthesis, X-ray diffraction method, spectroscopic characterization (FT-IR, <sup>1</sup>H and <sup>13</sup>C NMR), antimicrobial activity, Hirshfeld surface analysis and DFT computations of novel sulfonamide derivatives. *J. Mol. Struct.* **2018**, *1161*, 122–137. [[CrossRef](#)]
45. Pople, J.A.; Schleyer, P.V.; Hehre, W.J.; Radom, L. *AB INITIO Molecular Orbital Theory*; John Wiley & Sons: Hoboken, NJ, USA, 1986.
46. DiCésare, N.; Belletête, M.; Marrano, C.; Leclerc, M.; Durocher, G. Conformational Analysis (ab Initio HF/3–21G\*) and Optical Properties of Symmetrically Disubstituted Terthiophenes. *J. Phys. Chem. A* **1998**, *102*, 5142–5149. [[CrossRef](#)]
47. Mackenzie, C.F.; Spackman, P.R.; Jayatilaka, D.; Spackman, M.A. CrystalExplorer model energies and energy frameworks: Extension to metal coordination compounds, organic salts, solvates and open-shell systems. *IUCr* **2017**, *4*, 575–587. [[CrossRef](#)] [[PubMed](#)]



© 2020 by the authors. Licensee MDPI, Basel, Switzerland. This article is an open access article distributed under the terms and conditions of the Creative Commons Attribution (CC BY) license (<http://creativecommons.org/licenses/by/4.0/>).